RESEARCH ARTICLE SUMMARY

NEUROSCIENCE

Dynamics of cortical dendritic membrane potential and spikes in freely behaving rats

Jason J. Moore,* Pascal M. Ravassard, David Ho, Lavanya Acharya, Ashley L. Kees, Cliff Vuong, Mayank R. Mehta*

INTRODUCTION: Neurons are large, tree-like structures with extensive, branch-like dendrites spanning >1000 μm, but a small ~10-μm soma (figure). Dendrites receive inputs from other neurons, and the electrical activity of dendrites determines synaptic connectivity, neural computations, and learning. The prevailing belief has been that dendrites are passive; they merely send synaptic currents to the soma, which integrates the inputs to generate an electrical impulse, called an action potential or somatic spike, thought to be the fundamental unit of neural computation. These ideas have not been directly tested because traditional electrodes, which puncture the dendrite to measure dendritic voltages in vitro, do not work in vivo due to constant movement of the animals that kills the punctured dendrites. Hence, the voltage dynamics of distal dendrites, constituting the vast majority of neural tissue, is unknown during natural behavior.

RATIONALE: Tetrodes are a bundle of four fine electrodes, commonly used for measuring somatic spikes from a distance, that is, extracellularly. Hence, they work well in freely behaving animals. However, tetrodes do not measure the membrane voltages of soma, let alone dendrites. Chronically implanted tetrodes also elicit a naturally occurring immune response, where glial cells encapsulate the tetrode and shield it from the extracellular medium. We tested the hypothesis that a segment of dendrite could get trapped between the tetrode tips before this glial encapsulation occurred (figure). This would enable us to measure the dendritic membrane voltage without penetrating it in freely behaving subjects.

RESULTS: Despite low success rate, we measured the putative, distal-dendritic membrane potential in freely behaving rats for long periods, up to 4 days. These data showed frequent occurrence of spikes that were quite different from somatic spikes, but they closely resembled the waveforms of spikes generated within the distal dendrites in vitro (figure). This finding was further confirmed by computational modeling. The glial seal mechanism was verified using immunohistochemistry, predicted shielding of extracellular spikes during the dendritic measurements, in vivo impedance spectroscopy, and modeling. The identity of the general cell type from which the dendrite spikes were measured was confirmed using the analysis of short-term plasticity, suggesting that most of the dendritic measurements were from pyramidal neurons. The dendritic spike rates, however, were fivefold greater than the somatic spike rates of pyramidal neurons during slow-wave sleep and 10-fold greater during exploration. The high stability of dendritic signals suggested that these large rates are unlikely to arise due to the injury caused by the electrodes. The data also showed large subthreshold membrane voltage fluctuations. Their magnitude was always larger than that of dendritic spikes. This is the converse of comparable measurements in the soma. The dendritic spikes and subthreshold voltages contained significant information about the rat's exploratory behavior, which is comparable to somatic spikes.

ON OUR WEBSITE

Read the full article at http://dx.doi.org/10.1126/science.aaj1497

CONCLUSION: The glial sheath method can be used for measuring dendritic membrane potential in freely behaving animals for long periods. The large subthreshold voltage fluctuations in dendrites, which modulate the dendritic firing rates, indicate a hybrid, analog-digital code in the dendrites. These dendritic dynamics could profoundly influence synaptic plasticity and neural computations. The dendrites generated several-fold more spikes than the soma. The large dendritic spike rates could be responsible for the seemingly weak correlations between the somatic spikes across neurons. This requires a revision of many prevailing beliefs, for example, the dendrites are largely passive in vivo, and the somatic spike is the fundamental unit of neural computation. ■

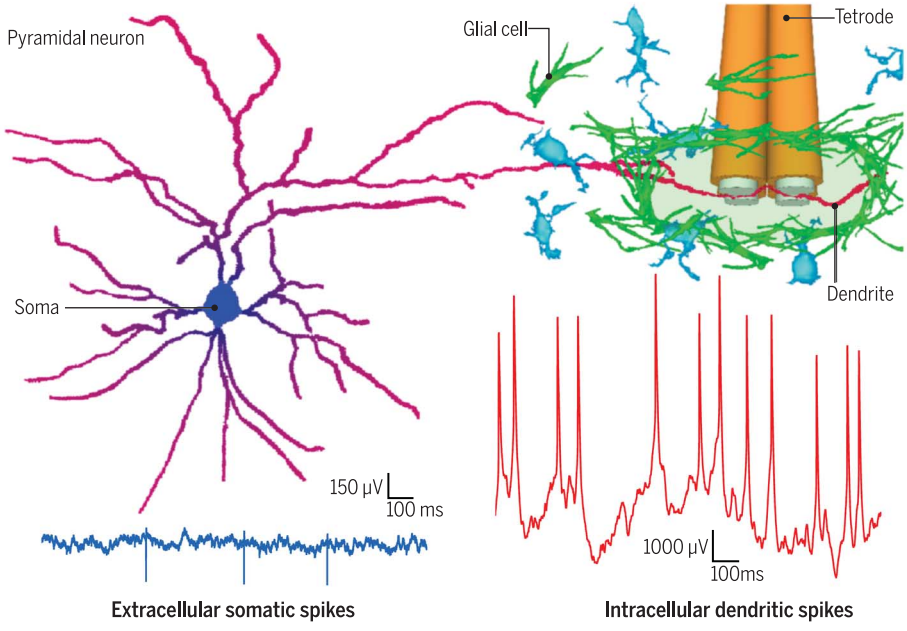

Glial sheath mechanism of measuring dendritic membrane potential in vivo. The top left shows a pyramidal neuron with soma (blue) and extensive dendrites (red). The top right shows the tetrode (gold) and glial cells (green) that trap a dendritic branch. The bottom left shows the extracellular measurements from the soma (blue), displaying few, small-amplitude, downward-going spikes. The bottom right shows membrane potential from the dendrite, displaying many, large-amplitude, upward-going spikes.

The list of author affiliations is available in the full article online.
*Corresponding author. Email: jason.moore@ucla.edu (J.J.M.); mayankmehta@ucla.edu (M.R.M.)
Cite this article as J. Moore *et al.*, *Science* **355**, eaaj1497 (2017). DOI: 10.1126/science.aaj1497

RESEARCH ARTICLE

NEUROSCIENCE

Dynamics of cortical dendritic membrane potential and spikes in freely behaving rats

Jason J. Moore,[1,2]* Pascal M. Ravassard,[1,3] David Ho,[1,2] Lavanya Acharya,[1,4] Ashley L. Kees,[1,2] Cliff Vuong,[1,3] Mayank R. Mehta[1,2,3,5]*

Neural activity in vivo is primarily measured using extracellular somatic spikes, which provide limited information about neural computation. Hence, it is necessary to record from neuronal dendrites, which can generate dendritic action potentials (DAPs) in vitro, which can profoundly influence neural computation and plasticity. We measured neocortical sub- and suprathreshold dendritic membrane potential (DMP) from putative distal-most dendrites using tetrodes in freely behaving rats over multiple days with a high degree of stability and submillisecond temporal resolution. DAP firing rates were several-fold larger than somatic rates. DAP rates were also modulated by subthreshold DMP fluctuations, which were far larger than DAP amplitude, indicating hybrid, analog-digital coding in the dendrites. Parietal DAP and DMP exhibited egocentric spatial maps comparable to pyramidal neurons. These results have important implications for neural coding and plasticity.

Microelectrode techniques have enabled the long-term measurement of extracellular somatic action potentials in freely behaving subjects. However, somatic action potentials are brief (~1 ms), occur rarely (~1.5 Hz in principal neocortical neurons), and only represent the binary output of neurons, whereas the vast majority of excitatory synapses are localized on their dendritic arbors, each spanning more than 1000 μm (*1*). In vitro studies show that dendrites support local spike initiation of dendritic action potentials (DAPs) (*2*–*16*) and back-propagating action potentials (bAPs) initiated at cell somata (*5*–*8*, *12*, *13*, *15*–*22*). Measurements in anesthetized, head-fixed animals (*23*–*26*) support these findings. DAPs affect synaptic integration (*16*, *27*–*33*) and endow neurons with greater computational power and information capacity (*14*–*16*, *29*, *30*, *32*–*38*) by turning dendritic branches into computational subunits with branch-specific plasticity (*9*–*11*, *14*–*16*, *30*–*32*).

Two-photon calcium imaging (*21*, *26*, *39*, *40*), sharp electrode (*2*), or patch-clamp techniques (*41*) can be used to study dendrites in vivo. However, calcium imaging is not a direct measure of subthreshold membrane potential or dendritic sodium spikes and lacks submillisecond resolution. Sharp electrode and patch-clamp techniques damage or rupture the membrane, thus limiting the recording duration (*42*) and altering in vivo neural dynamics, including firing rates (*43*); they are ill suited to record from thin dendrites. In addition, these methods often require the subject to be anesthetized or immobilized, which alter neural dynamics and limit possible behavioral paradigms.

Extracellular recording techniques can also, at times, record intracellular-like signals. Sharp glass pipettes occasionally measure "quasi-intracellular" somatic recordings in anesthetized animals (*44*–*48*). These recordings can be stable for, at most, a few hours (*45*), and the recorded spikes have identical shapes as somatic action potentials (width, ~1 ms) (*45*, *47*, *48*). Quasi-intracellular recordings are proposed to arise from a region of high electrical resistance, electrically isolating the membrane under the microelectrode, resulting in large-amplitude, intracellular-like signals. Microelectrode arrays can achieve an "in-cell" recording configuration (*49*, *50*) when cultured neurons engulf the recording electrodes, yielding a large seal resistance and allowing measurement of the intracellular voltage.

How might these phenomena be leveraged to investigate dendritic activity in vivo? We used chronically implanted tetrodes (see methods) (*51*, *52*), which are often flexible and have a narrow profile, to mitigate cell damage. Astrocytes and microglia can form a high impedance sheath around a tetrode and shield off the rest of the extracellular space (*53*–*55*). We hypothesized that this process can encapsulate a dendrite alongside the tetrode such that the voltages at the tetrode tips approximate the intracellular dendritic membrane potential (DMP) without penetrating the dendrite.

We implanted nine rats with hyperdrives containing up to 22 individually adjustable tetrodes, as described previously (see methods) (*51*, *52*). Tetrodes usually recorded standard extracellular signals, including thin (<1 ms) extracellular spikes of negative polarity with ~100-μV amplitude (Fig. 1A), presumably of somatic origin (*56*). However, in several instances [25 recordings made over 194 total tetrodes (13% success rate) in 21 of 847 total recording days (2% of recording sessions) across nine rats, see methods], the signal was markedly different, resembling an intracellular dendritic recording (Fig. 1B and movie S1). These signals manifested overnight, while all tetrodes were stationary. Here, the signal amplitude was orders of magnitude larger, containing broad (>5-ms base width) positive-polarity spikes with amplitudes of the order of thousands of microvolts (Fig. 1, B and C). These signals could be discerned only when the data acquisition system settings with high dynamic range were used. These measurements were obtained at a median of 18 (between 6 and 55) days after surgery and discontinuation of any psychoactive drug, ruling out any possible effects of anesthesia.

DAP versus extracellular spikes

For reasons described below, we refer to these spikes as DAP. We computed several features of the 25 DAP sources measured in vivo (Fig. 1D; see methods) and compared these to extracellular somatic spike measurements from 754 units across nine rats in vivo (Fig. 1, E to G) and to available intracellular reports of dendritic spiking (table S1) (*3*, *6*–*8*, *13*, *20*). First, similar to in-cell and quasi-intracellular measurements (*45*, *46*, *49*, *50*), DAP amplitude was always positive (850 μV; 25 to 75% range, 570 to 2100 μV) (Fig. 1, D and E, and fig. S1), in contrast to extracellularly recorded somatic spikes simultaneously recorded from nearby tetrodes; these were of negative polarity and of much smaller amplitude (−80 μV; 25 to 75% range, −50 to −110) (Fig. 1E and fig. S1). DAP rise time (0.57 ms; 25 to 75% range, 0.48 to 0.68 ms) was consistent across all recordings, similar to dendritic sodium spikes in vitro, and much larger than the rise time of the extracellular spikes (0.31 ms), but much faster than the rising phase of calcium spikes (Fig. 1, D and F, and table S1) (*3*, *8*, *20*, *39*). The full-width at half maximum (half-width) of DAP (4.3 ms; 25 to 75% range, 2.7 to 6.3 ms) (Fig. 1, D and G) was much longer than the DAP rise time (fig. S2, A and B) and far greater than the half-width of extracellular (0.26 ms; Fig. 1G) or intracellular (~0.7 ms; table S1) somatic spikes; DAPs were much wider than reported "high-amplitude positive spikes" from cortex (*57*) and somatic spikes recorded quasi-intracellularly (*44*–*48*). However, DAP half-width was much smaller than the typical half-width of dendritic calcium spikes (table S1). DAP width was more variable both within and across recordings (fig. S2), in

[1]W. M. Keck Center for Neurophysics, Integrative Center for Learning and Memory, and Brain Research Institute, University of California, Los Angeles, Los Angeles, CA 90095, USA. [2]Neuroscience Interdepartmental Program, University of California, Los Angeles, Los Angeles, CA 90095, USA. [3]Department of Physics and Astronomy, University of California, Los Angeles, Los Angeles, CA 90095, USA. [4]Biomedical Engineering Interdepartmental Program, University of California, Los Angeles, Los Angeles, CA 90095, USA. [5]Departments of Neurology and Neurobiology, University of California, Los Angeles, Los Angeles, CA 90095, USA.
*Corresponding author. Email: jason.moore@ucla.edu (J.J.M.); mayankmehta@ucla.edu (M.R.M.)

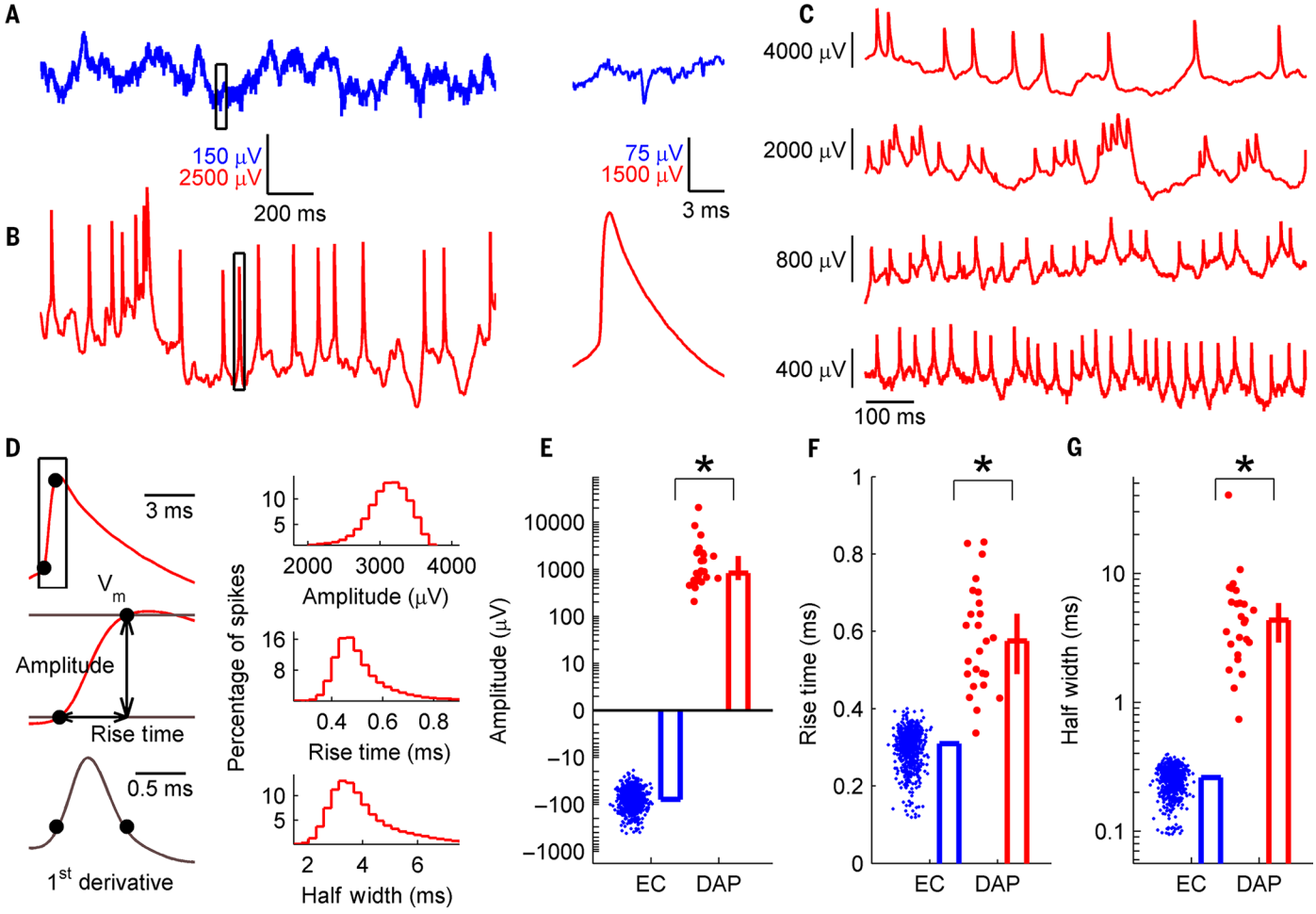

Fig. 1. Measurements of DAP in vivo. (**A**) Typical extracellular LFP showing ~100-μV fluctuations. Somatic action potentials are visible as thin, ~100-μV, negative-polarity spikes (inset to right). (**B**) Putative DMP recording on the same tetrode presented in (A) on the following day. Fluctuations are ~5000 μV. DAPs are visible as broad, positive-polarity, ~5000-μV spikes with a much longer falling phase than rising phase (inset to right). See also movie S1. (**C**) Sample membrane potential traces from four separate tetrodes, each exhibiting spontaneous dendritic spiking. (**D**) (Left) Quantification of DAP shape parameters (see methods). (Top right) Distribution of DAP amplitudes within a single recording session [3120 μV (3110 to 3130 μV); n = 8187 spikes]. (Middle right) Distribution of DAP rise times for the same recording session [0.49 ms (0.49 to 0.49 ms); n = 8187 spikes]. (Bottom right) Distribution of DAP half-widths for the same recording session [3.81 ms (3.78 to 3.84 ms); n = 8187 spikes]. (**E**) Extracellular spike amplitude (EC; blue) was always negative [−77.5 μV (−81.1 to −73.4 μV); n = 754 units], in comparison to DAPs (red) that were always positive [835 μV (597 to 1900 μV); n = 25 dendrites], and more than 10 times larger in magnitude ($P = 1.7 \times 10^{-17}$, Wilcoxon rank sum test). (**F**) The rise time of DAP [0.58 ms (0.49 to 0.65 ms); n = 25 dendrites] was significantly larger ($P = 1.7 \times 10^{-17}$, Wilcoxon rank sum test) than that of extracellular spikes [0.31 ms (0.31 to 0.31 ms); n = 754 units]. (**G**) The half-width of DAP [4.33 ms (2.92 to 5.90 ms); n = 25 dendrites] was also significantly larger ($P = 1.7 \times 10^{-17}$, Wilcoxon rank sum test) than that of extracellular spikes [0.26 ms (0.26 to 0.26 ms); n = 754 units]. Data are reported and presented as median and 95% confidence interval of the median. *$P < 0.05$.

contrast to very consistent DAP rise times across the data, and the two were significantly correlated ($r = 0.57$, $P = 0.003$) between DAP rise time and width across the recordings (fig. S2F). These differences in the variability of rise time and width across DAP are also characteristic of dendritic sodium spikes (table S1) (*3*, *6*–*8*, *17*, *20*, *21*, *26*, *39*).

Mechanism of DMP measurement: Glial sheath hypothesis

We hypothesized that the DMP recordings were achieved by combining the above-mentioned in-cell (quasi-intracellular) recording (*45*, *46*, *49*, *50*) and glial sheath mechanisms (*53*, *54*). Each tetrode bundle was ~35 to 40 μm in diameter, with a ~5-μm gap between the tips. An intact dendrite, only a few micrometers thick (*1*, *8*), could thus be caught in this gap, and the tetrode would record an intracellular dendritic signal once the glial sheath formed. Immunohistochemistry of cortical sections previously implanted with tetrodes (see methods) showed reactive astrocytes and microglia surrounding the tetrode location, with intact dendrites nearby (fig. S3A and movie S2). Increased resistance from the electrode tips to ground due to this encapsulation would allow recording of the intracellular membrane potential (fig. S3B). We performed impedance spectroscopy measurements on electrodes during either DMP or local field potential (LFP) recordings (fig. S3C). Fitting parameters to an electric circuit equivalent model of glial encapsulation (*55*, *58*), the only parameter that was significantly higher ($P = 1.8 \times 10^{-3}$) for DMP-recording electrodes, was the resistance between the electrode tip and ground, through the glial sheath (fig. S3, C and D). The estimated glial resistance was more than sixfold larger for DMP-recording electrodes compared to LFP-recording electrodes; this is precisely the condition predicted by the model that would yield glial sheath–assisted measurements of the intracellular voltage (fig. S3B).

Furthermore, we evaluated tetrode signal properties in the session before a DAP was recorded (PRE), during DAP recording (DUR), and in the session after the DAP signal was lost (POST). First, DAP amplitudes were nearly identical on all four channels of a tetrode in DUR (see methods),

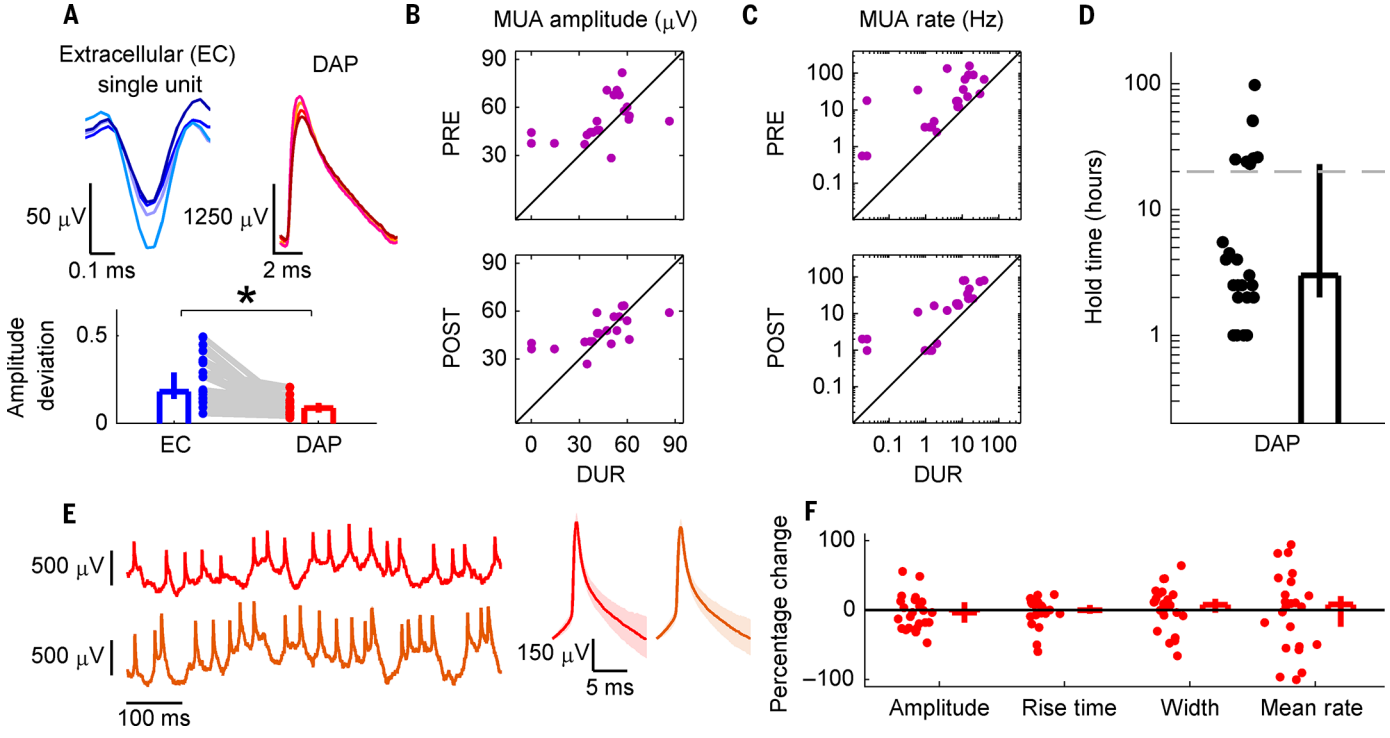

Fig. 2. DAP measurements are similar across all electrodes of a tetrode and are stable for long periods. (**A**) (Top) The waveform of a single extracellular spike has different amplitudes on each of the four tetrode channels (left), but the waveform of a single DAP on the same tetrode the following day has very similar amplitudes (right). (Bottom) The spike amplitude deviation across four electrodes (see methods) was significantly greater for extracellular single units recorded the day before DAPs were recorded (PRE) [0.18 (0.14 to 0.29); $n = 25$ units] compared to DAP during DMP recording (DUR) [0.09 (0.06 to 0.12); $n = 25$ DAP sources] on the same tetrode the following day ($P = 6.2 \times 10^{-6}$, Wilcoxon signed-rank test). (**B**) MUA amplitude during DMP recording (DUR) [41.8 μV (36.9 to 53.4 μV); $n = 25$ recordings] was significantly lower than during PRE [45.8 μV (44.3 to 54.6 μV); $n = 25$ recordings; $P = 6.6 \times 10^{-3}$, Wilcoxon rank sum test]. MUA amplitude was smaller in DUR compared to the day after DMP recording [POST; 44.1 μV (40.6 to 53.9 μV]; $n = 25$ recordings], but not significantly so ($P = 6.7 \times 10^{-2}$, Wilcoxon rank sum test). (**C**) MUA rate was significantly lower in DUR [5.19 (1.29 to 10.7); $n = 25$ recordings] compared to both PRE [17.5 Hz (4.84 to 34.7 Hz); $n = 25$ recordings; $P = 2.1 \times 10^{-5}$, Wilcoxon rank sum test] and POST [16.5 Hz (2.01 to 25.5 Hz); $n = 25$ recordings; $P = 8.0 \times 10^{-5}$, Wilcoxon rank sum test]. (**D**) DAP recordings were stable for long periods of time [3 hours (2 to 23 hours); $n = 25$ recordings], with the shortest recording lasting 1 hour and the longest lasting 97.5 hours. Durations between 5.5 and 23 hours are absent due to restrictions on total recording duration in a single day, resulting in artificial bimodality. Hence, all recording durations are likely an underestimate of actual duration for which the DAPs were held. (**E**) (Left) Membrane potential at the beginning of recording (top) and 90 min after (bottom) recording, showing little change in the quality of recording. (Right) Averaged DAP (median and 25th to 75th percentile) in the first part of the recording to the left ($n = 616$ DAP) compared to the averaged DAP in the later part of the recording ($n = 897$ DAP). (**F**) Percentage change from the first 5 min of recording to the last 2 min was not significantly different from 0 for amplitude [−3.48% change (−18.0 to 11.7% change); $n = 25$ dendrites; $P = 0.55$, Wilcoxon signed-rank test], rise time [0.00% change (−5.00 to 7.69% change); $n = 25$ dendrites; $P = 0.87$, Wilcoxon signed-rank test], half-width [7.76% change (−3.64 to 16.27% change); $n = 25$ dendrites; $P = 0.35$, Wilcoxon signed-rank test], or mean firing rate [7.93% change (−23.9 to 20.5% change); $n = 25$ dendrites; $P = 0.97$, Wilcoxon signed-rank test]. Data are reported and presented as median and 95% confidence interval of the median unless otherwise noted. $^*P < 0.05$.

unlike in the PRE condition where the voltages of extracellular spikes were different across the four channels (Fig. 2A). This would not occur if any single electrode of the tetrode had penetrated the dendrite, but would be expected if the dendrite and the entire tetrode tip were encapsulated during DMP recording. Second, this would result in the shielding off of the surrounding extracellular medium from the tetrode by the encapsulating glial sheath. In the DUR condition, both the amplitude and mean firing rate of detectable extracellular multiunit activity (MUA) were significantly reduced (Fig. 2, B and C; see methods) compared to PRE. In one case, one of four tetrode channels did not achieve an intracellular-like recording. MUA on only that channel was preserved, and its correlation with other channels remained low, suggesting that the single channel was not encapsulated by the glial sheath (fig. S4). Third, there was no evidence of damage to the tetrodes that yielded DMP measurements, because all MUA properties in POST were similar to those in PRE (Fig. 2, B and C).

DAP properties remained stable for long periods of time (Fig. 2, D to F). Our recordings typically lasted several hours, and DAP from the same tetrode could be recorded for up to 4 consecutive days (Fig. 2D; see methods). From the beginning to the end of the recording span of any single DMP, there was no systematic change in DAP amplitude, rise time, width, or mean firing rate (Fig. 2, E and F). These observations indicate that the tetrode did not damage the dendrite during these measurements (*42*, *43*, *59*, *60*).

Cellular identity of DAP

Although the rise times and widths of the spikes described above are consistent with dendritically generated sodium spikes, that is, DAP, they are also consistent with somatically generated spikes (bAP) (*6*–*8*, *12*, *13*, *15*–*22*). Hence, we compared the firing properties of DAP to those of extracellular somatic spikes recorded simultaneously on nearby tetrodes (see methods). We first examined data from slow-wave sleep (SWS) to minimize the influence of behavioral parameters (Fig. 3; see methods). DAP mean firing rates were high (7.1 Hz), more than fourfold greater than the mean firing rates of extracellular units (1.6 Hz) (Fig. 3, A and B). The high DAP firing rates were not due to multiple DAP sources being pooled together, because all DAP had interspike interval

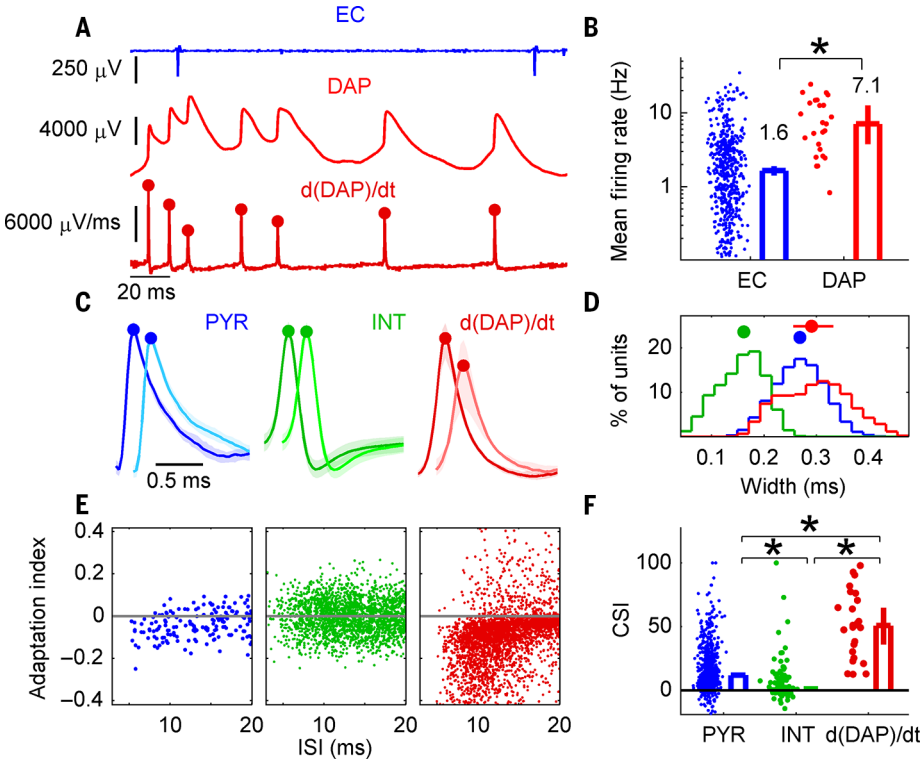

Fig. 3. DAPs are likely to be from pyramidal neurons but have much greater firing rates and stronger short-term plasticity. (**A**) (Top) Sample LFP showing a single extracellular unit firing at a relatively low rate. (Middle) Sample putative membrane potential showing a DAP firing at a higher rate. (Bottom) First temporal derivative of the membrane potential trace. Red dots indicate the peak value of identified DAP. Note activity-dependent attenuation. (**B**) In SWS, the mean spontaneous firing rate of extracellularly recorded units [1.65 Hz (1.41 to 1.91 Hz); n = 754 units] was more than fourfold smaller ($P = 4.1 \times 10^{-8}$, Wilcoxon rank sum test) than the firing rate of DAP [7.07 Hz (3.76 to 12.6 Hz); n = 25 dendrites]. Notice the near-complete absence of low (<1 Hz) DAP firing rate. (**C**) Demonstration of extracellular waveforms. The median and 25th to 75th percentile of sample pyramidal neuron (PYR; blue, n = 140 spike pairs), interneuron (INT; green, n = 6987 spike pairs), and d(DAP)/dt (red; 130 spike pairs) waveforms are plotted for the first spike (darker color) and the second spike in burst pairs (lighter color). PYR and DAP are broad, and the second spike has a smaller amplitude. This is not the case for INT. (**D**) Extracellular spike widths of PYR [0.27 ms (0.26 to 0.27 ms); n = 657 units] and DAP [0.29 ms (0.25 to 0.33 ms); n = 25 dendrites] were significantly greater than the extracellular spike width of INT [0.16 ms (0.15 to 0.17 ms); n = 97 units; PYR versus INT, $P = 1.2 \times 10^{-52}$; DAP versus INT, $P = 5.1 \times 10^{-14}$, Wilcoxon rank sum test for both]. DAPs were also significantly wider than PYR ($P = 1.5 \times 10^{-2}$, Wilcoxon rank sum test). (**E**) Adaptation index (see methods) plotted against ISI for a sample pyramidal neuron, interneuron, and DAP. For PYR and DAP, but not INT, the adaptation index is largely negative for ISI less than 20 ms. For clarity, every fifth spike pair is plotted for INT and DAP. (**F**) PYR CSI [12.0 (10.3 to 13.5); n = 657 units] was significantly greater ($P = 1.0 \times 10^{-11}$, Wilcoxon rank sum test) than that of INT [1.02 (0.25 to 2.99); n = 97 units], but smaller ($P = 2.9 \times 10^{-10}$, Wilcoxon rank sum test) than that of DAP [50.8 (36.0 to 65.0); n = 25 dendrites]. DAP CSI was significantly greater ($P = 4.7 \times 10^{-12}$, Wilcoxon rank sum test) than that of INT. Data are reported and presented as median and 95% confidence interval of the median unless otherwise noted. *P < 0.05.

(ISI) and amplitude distributions inconsistent with multiple independent sources (fig. S5; see methods). The high rates were also unlikely to be due to damage or otherwise altered activity of dendrites because of the longevity of recording (Fig. 2D) and the absence of any systematic changes in DAP kinetics or rate (Fig. 2, E and F) over long periods of time.

Could the high DAP rates be a result of preferentially recording from high-rate interneurons (*61*)? Interneurons have narrow spikes that exhibit very little spike amplitude attenuation within high-frequency bursts, characterized by very low complex spike index (CSI) (see methods) (*51*, *61*–*64*). In contrast, pyramidal neurons have wide spikes that exhibit consistent amplitude attenuation. These distinctions between cell types are present in dendrites as well (*8*, *16*, *18*, *19*, *65*, *66*). Thus, DAP should have wide spikes and a high CSI if recorded from pyramidal neurons.

We separated the extracellular units into putative pyramidal neurons and interneurons using standard methods (fig. S6A) (*61*) and compared their widths and CSI to the first temporal derivative of DAP, as an approximation of the extracellular waveform (*56*, *67*). Our data set contained far more pyramidal neurons (87%) than interneurons (13%). As expected, pyramidal neurons had significantly lower firing rates and larger widths and CSI than the interneurons (Fig. 3, C to F, and fig. S6B) (*61*, *62*, *68*). The estimated extracellular widths of DAP were slightly larger than pyramidal neurons but about twice as large as interneurons (Fig. 3D). The DAP CSI was slightly greater than that of pyramidal neurons but 50-fold greater than that of interneurons (Fig. 3, E and F). The distributions of both of these DAP measures were unimodal and most similar to pyramidal neurons, indicating that our DAPs were measured from the dendrites of pyramidal neurons.

DAP mean rate was significantly greater (more than fivefold) than that of pyramidal neurons ($P = 1.3 \times 10^{-9}$) (fig. S6B), as was the peak firing rate (DAP, 93.5 Hz; pyramidal, 67.6 Hz; $P = 1.0 \times 10^{-2}$; fig. S6C, only ~40%). The differential pattern of the mean and peak rates might be explained by the differences in short-term plasticity (*62*), which is greater in the pyramidal neuron dendrites compared to soma (*18*, *19*). This is manifested in activity-dependent adaptation of DAP amplitude, rise time, and width, similar to those in pyramidal neuron dendrites in vitro (fig. S6, D and E) (*18*, *19*).

To determine whether these are bAP or DAP and the locus of their measurement, we compared our experimental results with the simulations of a multicompartment model of cortical layer 5 pyramidal neuron (fig. S7) (*69*–*73*). The rise time and widths of our data had a significant overlap with those of simulated DAP generated in the distal-most dendrites and measured locally (fig. S7, B and D). In contrast, these measured parameters had only a partial overlap with the bAP (fig. S7, C and D). These results suggest that for the case of layer 5 pyramidal neurons, most of our measured DAPs are locally generated and measured in the distal-most dendrites. Similar results may hold for other pyramidal neuron types and dendrites. This hypothesis is further supported by the observation that DAP rates are several-fold greater than somatic rates (Fig. 3B and fig. S6B).

Further analysis of DAP properties did not show evidence of two different populations. The DAP rates were similar at all depths (from 330 to 1240 μm; P = 0.24; fig. S8A) and were greater than somatic rates at all depths (fig. S8B). Other properties of DAP sources were uncorrelated with DAP rate as well, including amplitude (P = 0.19), rise time (P = 0.14), half-width (P = 0.49), and CSI (P = 0.57) (fig. S8C), suggesting no clear demarcation between high- and low-rate DAP. The disparately large rates of DAP compared to somatic spikes suggest that only a fraction of DAPs elicit somatic spiking, indicating a significant decoupling of dendrites and somata (*2*, *5*, *6*, *8*, *19*, *31*, *32*).

Subthreshold dendritic potential dynamics during SWS

Subthreshold fluctuations accompanying DAP during SWS had characteristics suggesting that they represent the DMP (Fig. 4A; see methods). The subthreshold fluctuations were of the order

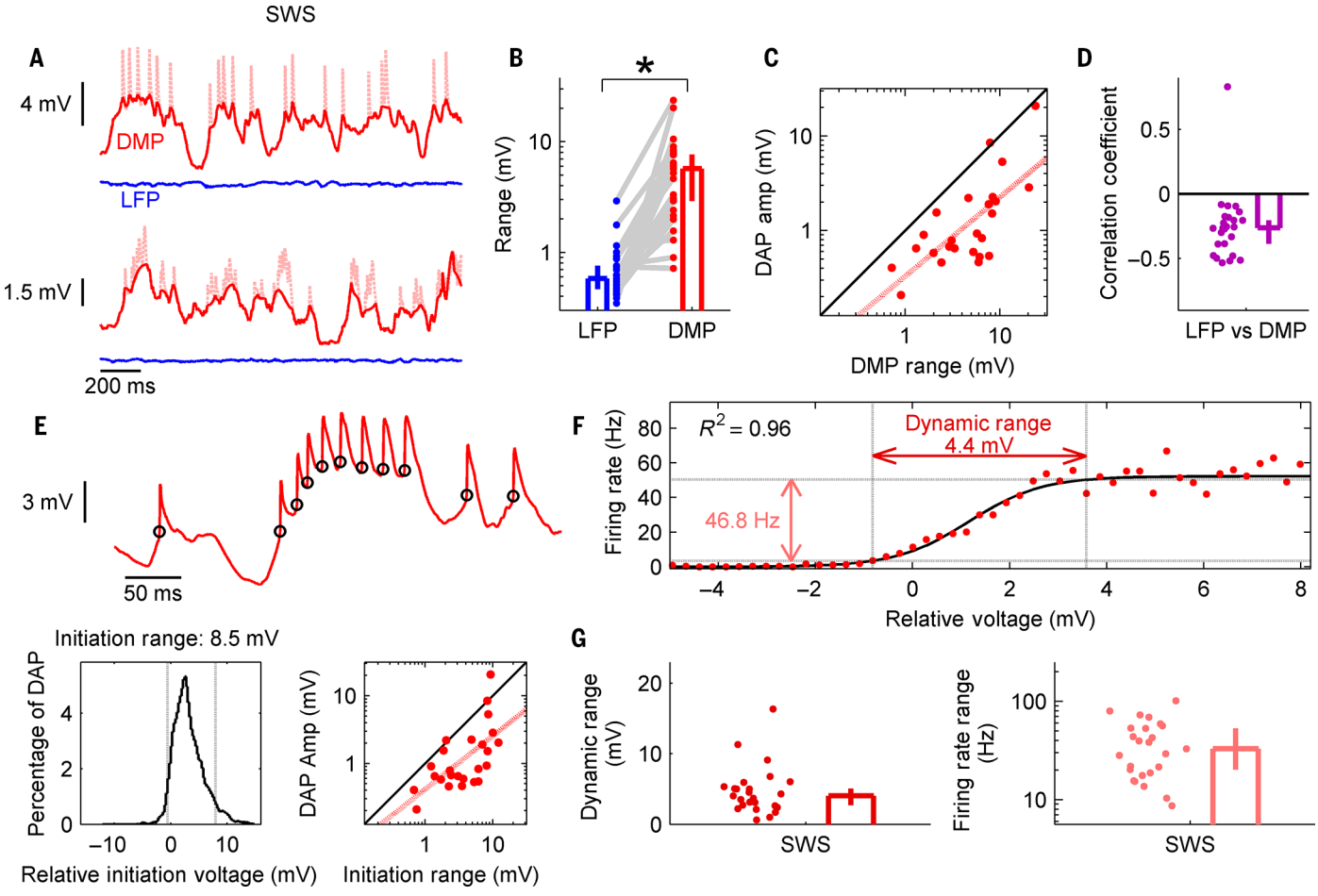

Fig. 4. Large subthreshold membrane potential fluctuations modulate DAP rates during SWS. (**A**) (Top) Sample DMP (red) trace during SWS, showing prominent oscillations of the same order of magnitude as DAP. DAPs are shown in light red to highlight the spike-clipped subthreshold membrane potential. Below on the same scale is the LFP (blue) recorded simultaneously on a nearby tetrode. (Bottom) Same as above but from a different pair of tetrodes in a different recording session. (**B**) The range of the LFP [0.58 mV (0.47 to 0.76 mV); n = 25 LFP] was nearly an order of magnitude (9.9-fold) smaller than the subthreshold DMP accompanying DAP [5.72 mV (2.92 to 7.69 mV); n = 25 dendrites]. *$P = 1.6 \times 10^{-8}$, Wilcoxon signed-rank test. (**C**) In SWS, the range of subthreshold DMP was nearly always larger ($P = 1.4 \times 10^{-5}$, Wilcoxon signed-rank test) than the corresponding DAP amplitude [0.84 mV (0.60 to 1.90 mV); n = 25 dendrites] and positively correlated [r = 0.71 (0.44 to 0.86); $P = 6.9 \times 10^{-5}$, two-sided t test). (**D**) In all but one case, LFP and simultaneously recorded DMP during SWS were negatively correlated [r = −0.26 (−0.38 to −0.20)]. See also movie S1. (**E**) (Top) Sample DMP trace segment showing a dynamic threshold for DAP initiation, with the initiation points marked by black circles. (Bottom left) Histogram of initiation voltages for the entire recording session from which the above was taken; the 5 to 95% range of initiation voltages spans 8.5 mV. (Bottom right) DAP initiation range [3.67 (2.24 to 6.99); n = 25 dendrites] was larger ($P = 5.1 \times 10^{-5}$, Wilcoxon signed-rank test) than the corresponding DAP amplitude and positively correlated [r = 0.63 (0.31 to 0.82); $P = 7.4 \times 10^{-4}$, two-sided t test]. (**F**) Sample DAP firing rate as a function of relative voltage, which was well approximated (fig. S9G) by a sigmoidal logistic function (black line). Firing rates here vary by 46.8 Hz over a dynamic range of 4.4 mV. (**G**) (Left) The population of DAP had a large dynamic range of initiation voltages [4.03 mV (2.74 to 5.07 mV); n = 25 dendrites], as defined in (F). (Right) The firing rate range of the DAP population was similarly wide [33.1 Hz (20.3 to 53.1 Hz); n = 25 dendrites]. Data are reported and presented as median and 95% confidence interval of the median.

of thousands of microvolts, reaching up to 20 mV (Fig. 4, A and B), far exceeding the range of the LFP on nearby tetrodes (Fig. 4B). The range of the subthreshold fluctuation was positively correlated with the DAP amplitude on the same recording (Fig. 4C). Nearby LFP range was not correlated with DAP amplitude (fig. S9A). These results could arise because of the quality of glial-sealed encapsulation (figs. S3 and S4). The subthreshold range was always greater (6.8-fold) than the corresponding DAP amplitude (Fig. 4C), a membrane property primarily observed in vitro in dendrites that are electrotonically distant from the soma (*3*, *5*–*8*, *20*, *23*–*25*). In all but one case, the DMP signal in SWS was significantly negatively correlated with the LFP signal on a nearby tetrode (Fig. 4D, fig. S9B, and movie S1), similar to somatic membrane results (*74*).

We next quantified the relationship between the instantaneous subthreshold DMP magnitude and DAP rate (see methods) (*75*). The range of subthreshold DMP at which DAP initiated was 4.4-fold larger than the magnitude of the corresponding DAP and positively correlated with DAP amplitude (Fig. 4E). The large DAP initiation range (Fig. 4E) is similar to that reported for dendrites in vitro (*3*, *5*–*8*, *20*, *25*), further supportive of the dendritic origin of our measurements.

Subthreshold DMP strongly modulated DAP rates. During SWS, DAP rate had a slowly increasing, sigmoidal dependence on subthreshold DMP (Fig. 4F), with the rate increasing over a large dynamic voltage range (see methods), which often exceeded the magnitude of DAP themselves (Fig. 4, F and G, and fig. S9C). The firing rate was modulated from nearly 0 Hz at low values of the

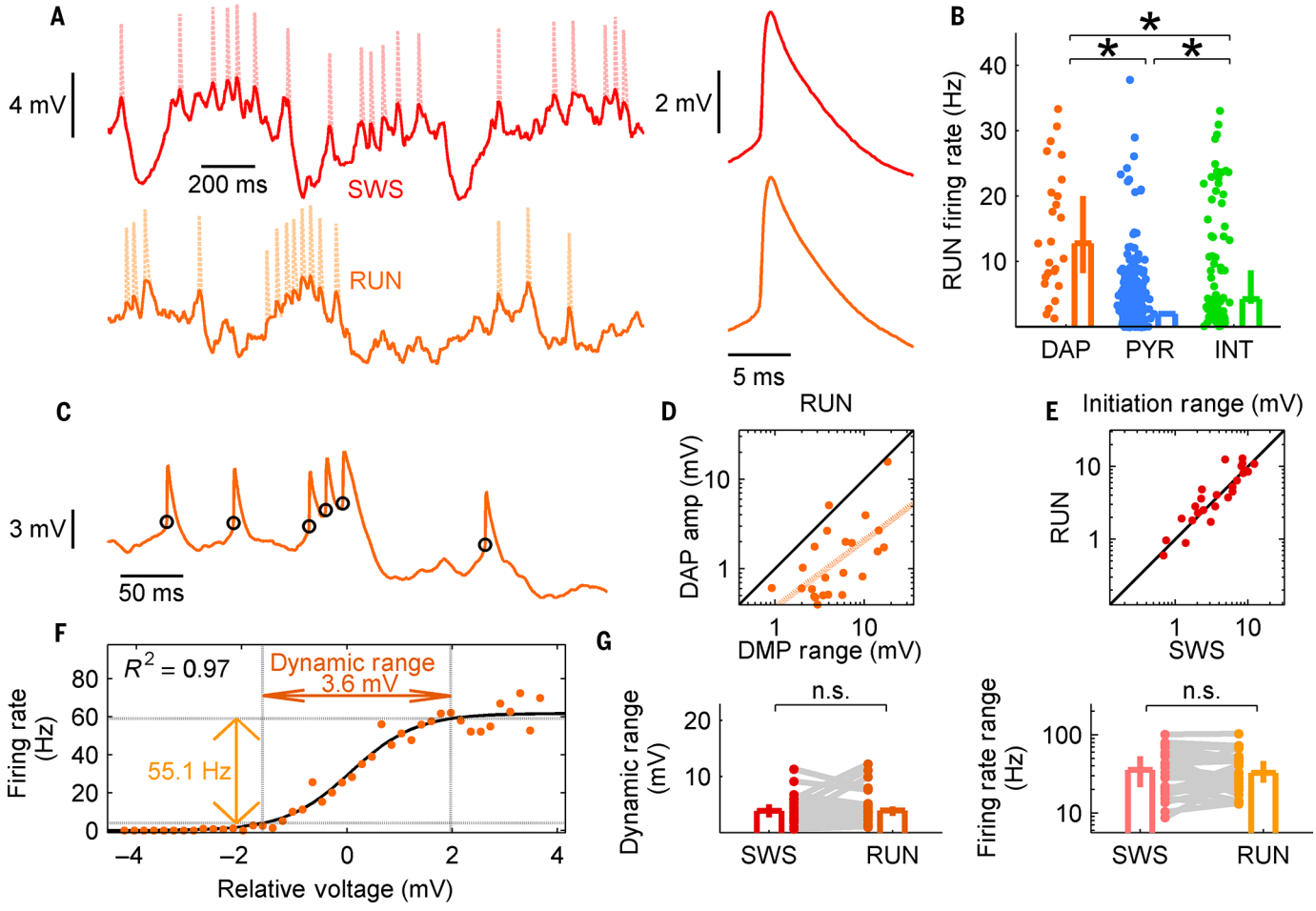

Fig. 5. Large subthreshold membrane potential fluctuations modulate DAP rates during RUN. (**A**) Sample membrane potentials during SWS (red; left) and locomotion (RUN; orange; right) show similar dynamics and amplitude of both DMP and DAP (middle). (**B**) DAP mean firing rate during RUN [12.8 Hz (8.29 to 20.0 Hz); n = 25 dendrites] was significantly greater than that of pyramidal neurons [1.99 Hz (1.63 to 2.37 Hz); n = 657 units; $P = 1.8 \times 10^{-5}$, Wilcoxon rank sum test] and interneurons [4.25 Hz (3.57 to 8.65 Hz); n = 97 units; $P = 8.3 \times 10^{-3}$, Wilcoxon rank sum test]. (**C**) Sample DMP trace during RUN shows a dynamic initiation range similar to that observed in SWS (Fig. 4E). (**D**) DMP range during RUN [3.82 mV (2.76 to 6.17 mV); n = 25 dendrites] was significantly larger ($P = 1.6 \times 10^{-5}$, Wilcoxon signed-rank test) than the corresponding DAP amplitude [0.82 mV (0.52 to 1.78 mV); n = 25 dendrites] and significantly correlated [r = 0.68 (0.39 to 0.85); $P = 2.0 \times 10^{-4}$, two-sided t test]. (**E**) DAP initiation ranges in SWS [3.67 mV (2.24 to 6.99 mV); n = 25 dendrites] and RUN [4.07 mV (2.51 to 8.14 mV); n = 25 dendrites] were positively correlated [r = 0.91 (0.80 to 0.96); $P = 3.4 \times 10^{-10}$, two-sided t test] and not significantly different (P = 0.46, Wilcoxon signed-rank test). (**F**) Sample V-R curve during RUN, which was well described (fig. S11) by a sigmoidal logistic function. (**G**) Twenty-four of 25 dendrites had sufficient data to characterize V-R curves in RUN. (Left) The dynamic voltage range during RUN [3.90 mV (2.98 to 4.67 mV); n = 24 dendrites] was not significantly different (P = 0.73, Wilcoxon signed-rank test) from the dynamic range in SWS [3.87 mV (2.74 to 5.03 mV); n = 24 dendrites]. (Right) The firing rate range in RUN [32.5 Hz (24.6 to 46.5 Hz); n = 24 dendrites] was not significantly different (P = 0.86, Wilcoxon signed-rank test) from the range during SWS [35.6 mV (21.6 to 53.1 mV); n = 24 dendrites]. Data are reported and presented as median and 95% confidence interval of the median. *P < 0.05; n.s., not significant.

membrane voltage up to above 100 Hz at the highest membrane voltages (Fig. 4, F and G, and fig. S9C). Because short-term ion channel dynamics could influence spike initiation properties (*75*), the above calculations were also done for only those DAPs that were separated from all others by at least 50 ms (termed solitary DAP), with only minor differences (fig. S9, D to H).

Dendritic sub- and suprathreshold membrane potential in freely moving rats

The stability of our recordings allowed us to compare dendritic activity and its subthreshold modulation between SWS and during spontaneous, free locomotion (RUN) (Fig. 5A; see methods). DAP mean rate during RUN (12.8 Hz) was nearly twice as large compared to the mean rate during SWS (6.87 Hz; Fig. 5B) and significantly greater than that of pyramidal neurons (1.99 Hz) or interneurons (4.25 Hz). There was no significant difference in the firing rates between slow and fast runs in DAP. DAP amplitude was slightly smaller during RUN compared to SWS (fig. S6, D and E), and rise time and width were slightly longer, though the difference in width was not statistically significant (Fig. 5, A and B).

Subthreshold DMP measures were also comparable in SWS and RUN. First, the magnitude of subthreshold DMP was equally large in the two conditions (Fig. 5A and fig. S10). This is in contrast to the LFP, where fluctuations are severely diminished during locomotion compared to the large fluctuations present in SWS (fig. S10) (*76*, *77*). The subthreshold DMP magnitude during locomotion was 4.7-fold larger than the corresponding DAP amplitude, and the two were highly correlated (Fig. 5, C and D), as in SWS. Second, DAP had a large initiation range in RUN (Fig. 5, C and E) that was fivefold larger than the corresponding DAP amplitude, as in SWS (fig. S11A). DAP rate during RUN was also modulated by subthreshold DMP in a sigmoidal fashion (Fig. 5, F and G, and fig. S11B) over a wide dynamic voltage range and spanned a large range of firing

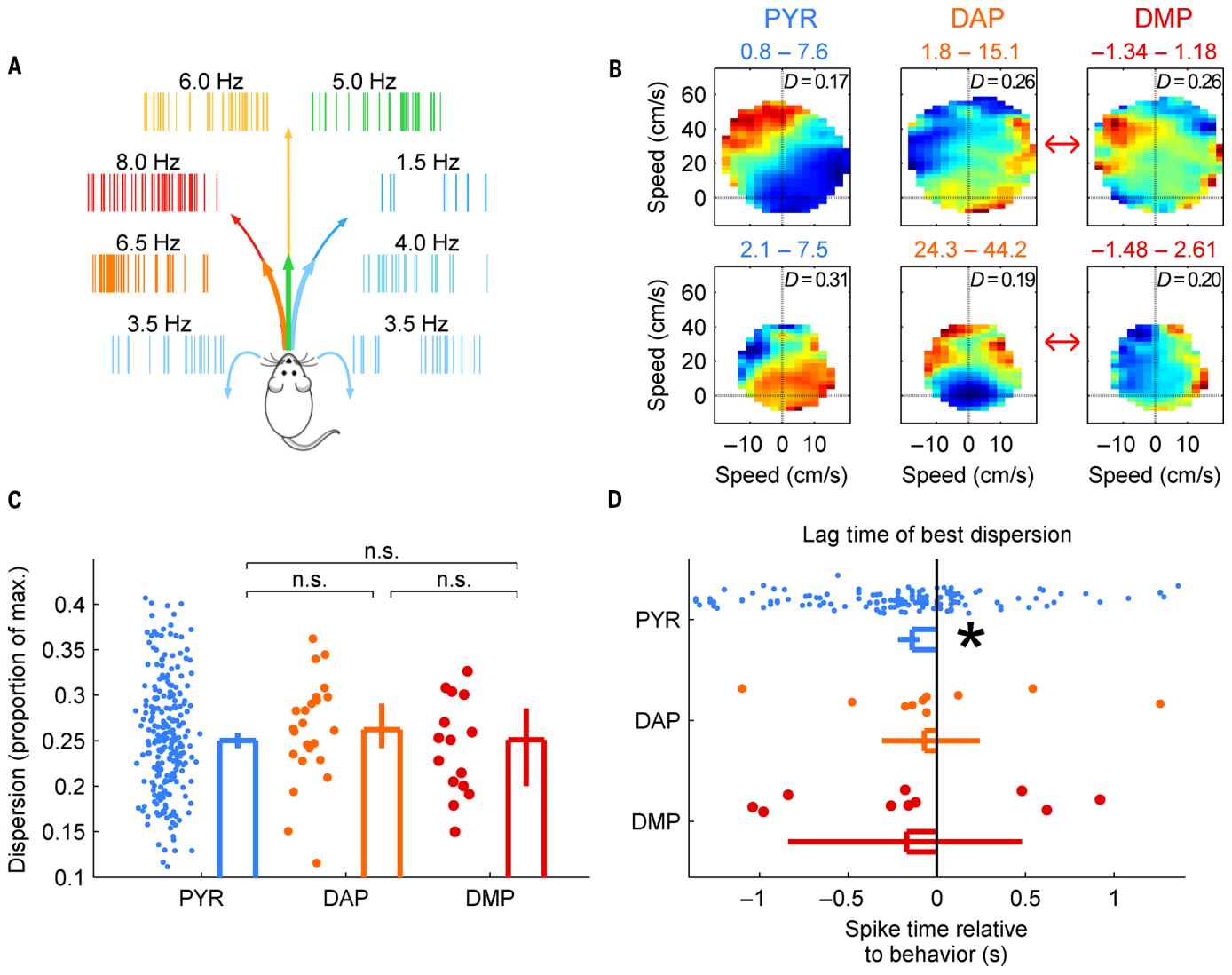

Fig. 6. DAP and DMP exhibit egocentric tuning comparable to somatic spikes. (**A**) Schematic of egocentric map computation. In this example, the neuron fires maximally (8 Hz, red) during a left-hand turn at high velocity and minimally (1.5 Hz, blue) during a right-hand turn at high velocity. (**B**) Two-sample pyramidal (PYR, left), DAP (middle), and DMP (right) egocentric maps. The minimum and maximum firing rates (mean voltages for DMP) for each map are displayed in the title, and the normalized dispersion *D* (see methods and fig. S10, A and B) is displayed in the upper-right corner. Red arrows indicate DAP and DMP from the same recording sessions. (**C**) The normalized dispersion (see methods) of PYR [0.25 (0.24 to 0.26); $n = 245$ maps] was not significantly smaller than that of DAP [0.26 (0.24 to 0.29); $n = 24$ maps; $P = 0.4$, Wilcoxon rank sum test] and DMP [0.25 (0.20 to 0.30); $n = 15$ maps; $P = 0.57$, Wilcoxon rank sum test]. DAP and DMP dispersions were not significantly different from each other ($P = 0.33$, Wilcoxon rank sum test). (**D**) The time lag corresponding to the optimal tuning for PYR with significant tuning [−140 ms (−220 to −100 ms); $n = 146$ maps with significant tuning] was significantly different from 0 ($P = 9.4 \times 10^{-7}$, Wilcoxon signed-rank test). The same measure for DAP [−70 ms (−310 to 240 ms); $n = 10$ maps with significant tuning] was not different from 0 ($P = 0.61$, Wilcoxon signed-rank test). DMP lag [−170 ms (−840 to 480 ms); $n = 10$ maps with significant tuning] was also not significantly different from 0 ($P = 0.43$; Wilcoxon signed-rank test) and not significantly different from either PYR ($P = 0.94$, Wilcoxon rank sum test) or DAP ($P = 0.5$, Wilcoxon rank sum test). Data are reported and presented as median and 95% confidence interval of the median. *$P < 0.05$; n.s., not significant.

rates, both of which were as large as in SWS (Fig. 5, F and G). These results were similar when performed on solitary DAP during locomotion (fig. S11, C to H).

Modulation of DAP, DMP, and soma by behavior

Do DAP and DMP contain information about instantaneous behavior? Previous studies have shown that somatic spike rates in the posterior parietal cortex (PPC) are modulated by specific types of movements, including forward running, left turns, and right turns (Fig. 6A) (*78*, *79*), and have an anticipatory component to their response (Fig. 6B and fig. S12A; see methods) (*78*). We computed the normalized dispersion, or spread, and depth of modulation of egocentric response maps for parietal DAP rate, subthreshold DMP voltage, and somatic spike rate (Fig. 6B and fig. S12A; see methods) during free locomotion in a rest box and a random foraging task (fig. S12B; see methods). The anticipatory component was quantified by finding the time lag corresponding to the best tuning (fig. S12C; see methods).

There were similar properties of egocentric tuning in pyramidal somata (PYR), DAP, and DMP (Fig. 6C). Normalized dispersion for PYR (0.25) was slightly but not significantly better than that for DAP (0.26; $P = 0.40$, Wilcoxon rank sum test) and DMP (0.25; $P = 0.571.4 \times 10^{-2}$, Wilcoxon rank sum test), which were also not significantly different from each other ($P = 0.33$, Wilcoxon rank sum test). The depth of modulation

of egocentric maps was comparable between all three groups (fig. S12D), with a similar percentage having a depth of modulation significantly above chance [PYR, 146 of 245, 60% (53 to 66%); DAP, 10 of 24, 42% (22 to 63%); DMP, 10 of 15, 67% (38 to 88%)]. Coherence showed a different pattern, with DMP having the highest coherence (fig. S12E), but this is likely an artifact because coherence is computed on unsmoothed rate maps, and the continuous DMP signal has more data than spiking point processes. Similar to dispersion, both short-term (fig. S12F) and long-term (fig. S12G) stability for PYR was larger than that for DAP and DMP, but the differences were not statistically significant.

The time lag corresponding to the optimal depth of modulation for pyramidal neurons with significant tuning was significantly negative (−140 ms, $P = 9.4 \times 10^{-7}$) (Fig. 6D) (*78*), indicating a preference to code for future movements. In some instances, somatic spikes were best tuned for behavior several seconds in the future or past (fig. S12H). The optimal lag time for significantly tuned DAP (−70 ms) and DMP (−170 ms) was not significantly different from 0 (DAP, $P = 0.50$; DMP, $P = 0.43$).

Hence, pyramidal neuron somata and dendrites both code for egocentric movement, but with differences that illustrate potential computational principles within a neuron. Pyramidal somatic responses are less dispersed than DAP and DMP responses, although equivalent percentages of PYR, DAP, and DMP are significantly tuned. The optimal coding occurs at negative time lags, or prospectively, for pyramidal somatic spikes but not for DAP or DMP.

Conclusions

We directly recorded the membrane potential and sodium spikes of putative neocortical distal dendrites in freely behaving rats without the confounding effects of recent anesthesia or restraint typically used with in vivo patch-clamp or optical imaging procedures. These measurements were done at submillisecond temporal resolution and were stable for at least 1 hour and up to 4 days. DAP kinetics were similar to those seen in vitro and in anesthetized animals (*3*, *5*–*8*, *20*, *23*–*25*). These recordings revealed a number of interesting properties of dendritic activity. First, DAP occurred at very high rates in vivo, far greater than somatic rates. Second, DAPs were accompanied by large subthreshold DMP fluctuations, the magnitudes of which were always larger than the DAP amplitude. Third, this was present not only during SWS but also during free locomotion. Fourth, DAP rates varied by an order of magnitude as a function of the subthreshold DMP in a graded fashion during both SWS and movement, suggesting a large dynamic range. Fifth, unlike previous reports (*26*, *39*), our measurements from PPC showed substantial differences between DAP, DMP, and somatic spikes in both quality and temporal dynamics.

Discussion

DAPs have long been hypothesized to endow neurons with greater computational power by turning dendritic branches into computational subunits with branch-specific plasticity (*14*–*16*, *29*–*37*). Dendrites support initiation and propagation of action potentials in vitro via voltage-gated sodium, potassium, and calcium channels (*3*, *5*–*8*, *16*, *20*, *27*–*32*). It has been unclear whether the conditions for generating DAP exist in vivo during natural behavior. Patch-clamp recordings in head-fixed mice suggest that proximal dendrites in visual cortex support spikes, though most of them were bAP and some were DAP (*26*). In contrast, our recordings are putatively from electrotonically distal-most dendrites, which generate dendritic spikes locally, and where somatically generated bAPs are mostly absent (*2*, *5*, *6*, *8*, *19*). These recordings were stable for hours or days at a time during free locomotion, with no evident damage to the dendrite.

We hypothesize that our tetrodes are in a "glial-assisted" configuration similar to in-cell or quasi-intracellular recordings (*45*, *46*, *49*, *50*). In this model, the requisite high-seal resistance comes from glial encapsulation (*53*, *54*) trapping a segment of a thin dendrite between the four electrode tips and the glial cells, forming a stable configuration, providing high-quality, positive-polarity, sub- and suprathreshold signals. Our immunohistochemical labeling and in vivo impedance spectroscopy measurements support this model, and the negative correlation between the subthreshold DMP and LFP is consistent with the whole-cell results from the soma (*74*). The encapsulation process might be facilitated by the fine-scale geometry of our gold-plated tetrode tips. However, the tetrodes have to be positioned close enough to a neuron to trap the dendrite without puncturing it. Our current success rate of dendritic recordings is quite low but comparable to the success rate of somatic whole-cell recordings during natural behavior (*60*, *80*, *81*).

Several signal properties, including dendritic spike rise time and width, firing rate, and short-term plasticity, are consistent with the hypothesis that our measurements are from the electrotonically distal-most dendrites of pyramidal neurons, and the dendritic spikes are generated locally in the dendrites, not back-propagated from the soma. The high DAP rates are unlikely to come from damage to the neuron due to stable DAP properties over hours. Spike properties, such as width and complex spiking, indicate that our data are from the pyramidal neurons but not from inhibitory interneurons. This may be because less than 20% of neurons are interneurons and their dendritic arbor is far smaller than that of pyramidal neurons, thus reducing the chances of encountering interneurons. The dendritic spike properties were unimodal, with low variability and no refractory violations, indicating a single dendritic source. Although many dendrites could be potentially trapped between the tetrode tips, very few would remain intact, reducing the success rate and the chance of recording multiple sources. This is consistent with recording two order of magnitude less (than expected) extracellular cells using tetrodes (*56*).

Because these rates greatly exceed those of pyramidal units in the same brain region, a large amount of activity and information processing in a neuron may be occurring in the dendrites without being read out in the postsynaptic soma, consistent with in vitro studies showing decoupling of somatic and dendritic compartments (*2*, *5*, *6*, *8*, *11*, *19*, *31*, *32*). The results of DAP computations could travel to the rest of the network via second messengers and presynaptic mechanisms. The semi-independence of distal dendrites suggests that *N*-methyl-D-aspartate–dependent plasticity, which crucially depends on depolarization, could be induced in only a specific dendritic branch, allowing for more input-specific plasticity and clustering of synapses with similar information (*11*, *14*, *33*–*37*) and greatly expanding the computational capacity of a single neuron.

DAP firing rates are modulated in a graded fashion by the subthreshold DMP. This endows the dendrites with an analog code, defined by the depolarization level of the dendrite, reminiscent of the sigmoidal response profile of the hidden layer of artificial neural networks (*34*, *35*). The digital coding, carried out by DAP, coexists with the subthreshold modulation, indicating a hybrid, analog-digital code in the dendrites. This large subthreshold modulation range (average, ~5 mV; maximum, ~20 mV) is consistent with but greater than recent results from the somata of hippocampal CA1 neurons (*59*, *60*, *81*), entorhinal stellate cells (*82*), and barrel cortex neurons (*83*). The true subthreshold voltage range in our case is likely even greater, because the magnitude of signals obtained through our measurement technique would be smaller than the true range and influenced by the quality of the glial seal. Our modeling results suggest that DAPs are measured at a distance from the site of initiation. Hence, local subthreshold fluctuations and variable propagation efficacy could result in variation in DAP peak voltage.

Somatic spikes in PPC are modulated by movement in an egocentric reference frame (*79*) in an anticipatory fashion during free behavior (*78*). DAP and DMP also exhibit egocentric modulation, but are more disperse and do not show significant anticipatory behavior. Our findings suggest a computational framework in which individual cortical neurons take information about the current state of the world, present in the dendrites, and form an anticipatory, predictive response at the soma, a computation similar to that performed by a Kalman filter (*84*) or hidden Markov model (*85*). Unlike network models of sequence learning, each individual neuron may behave like a feed-forward circuit that performs predictive coding based on nonpredictive inputs arriving from many dendritic branches (*36*, *86*, *87*). The intermediate integration step performed by the dendrites is likely a crucial one in neurons with extensive dendritic trees to allow inputs at distal tufts to be integrated in the somatic response (*5*).

These results demonstrate that dendrites generate far more spikes than the soma. This has important implications in many fields. The total energy consumption in neural tissue, measured in functional magnetic resonance imaging studies, could be dominated by the dendritic spikes

(*88*). Correlations between neuronal somatic spikes may be weak (*89*) due to the larger number of dendritic spikes, with only a fraction generating somatic spikes, possibly owing to inhibitory synapses interrupting propagation. Thus, the abundance of digital dendritic spikes and large analog subthreshold fluctuations in vivo could profoundly alter synaptic plasticity, altering the nature of neural coding and memory. This hybrid, analog-digital code in a dendrite, generated by a local cluster of excitatory synapses (*36*), may be the fundamental building block of neural information processing.

Methods summary

Data were obtained from nine adult male Long-Evans rats. The animals were food- and water-restricted. They received sugar water or solid cereal rewards during spatial exploration tasks, while their spatial position was monitored using an overhead camera. Rats were implanted with independently adjustable NiChrome tetrodes targeting prefrontal cortex and/or posterior parietal cortex. All methods were analogous to procedures described previously (*51*, *52*) and in accordance with NIH approved protocols. Neural signals were recorded continuously using the Neuralynx data acquisition system and screened for intracellular-like signatures (e.g., broad, large-amplitude spikes of reverse polarity compared with extracellular units). Putative DAP were identified as positive peaks in the intracellular-like signal that exceeded noise threshold (fig. S1). Movement in an egocentric reference frame was computed frame by frame by calculating the difference in position and heading direction between the start and end of a moving time window (*78*). In vivo impedance spectroscopy was done during extracellular recording and DAP recording separately and fitted with a biophysical model to estimate the putative glial seal parameters. Upon the completion of experiments, brains were extracted and immunohistochemistry performed (fig. S3).

Compartmental modeling (fig. S7) was performed in NEURON version 7.2 (*70*) using a modification of a previously published model of a layer V pyramidal neuron (*69*). Tests of significance between unpaired data or paired data were conducted using the Wilcoxon rank-sum test or Wilcoxon signed-rank test, respectively. Unless otherwise stated, all values are reported as median and 95% confidence interval of the median, estimated using resampling statistics. All analyses were done offline using custom-written codes in MATLAB. Details of experimental methods, analyses, and modeling can be found in the supplementary materials (*51*, *52*).

REFERENCES AND NOTES

1. S. Ramón y Cajal, *Histologie du Systeme Nerveux de l'Homme and des Vertebres* (Rue de l'Ecole-de-Medecine, 1909).
2. W. A. Spencer, E. R. Kandel, Electrophysiology of hippocampal neurons: IV. Fast prepotentials. *J. Neurophysiol.* **24**, 272–285 (1961). pmid: 25286477
3. Y. Amitai, A. Friedman, B. W. Connors, M. J. Gutnick, Regenerative activity in apical dendrites of pyramidal cells in neocortex. *Cereb. Cortex* **3**, 26–38 (1993). doi: 10.1093/cercor/3.1.26; pmid: 8439739
4. M. London, A. Schreibman, M. Häusser, M. E. Larkum, I. Segev, The information efficacy of a synapse. *Nat. Neurosci.* **5**, 332–340 (2002). doi: 10.1038/nn826; pmid: 11896396
5. T. Jarsky, A. Roxin, W. L. Kath, N. Spruston, Conditional dendritic spike propagation following distal synaptic activation of hippocampal CA1 pyramidal neurons. *Nat. Neurosci.* **8**, 1667–1676 (2005). doi: 10.1038/nn1599; pmid: 16299501
6. T. Nevian, M. E. Larkum, A. Polsky, J. Schiller, Properties of basal dendrites of layer 5 pyramidal neurons: A direct patch-clamp recording study. *Nat. Neurosci.* **10**, 206–214 (2007). doi: 10.1038/nn1826; pmid: 17206140
7. M. E. Larkum, J. Waters, B. Sakmann, F. Helmchen, Dendritic spikes in apical dendrites of neocortical layer 2/3 pyramidal neurons. *J. Neurosci.* **27**, 8999–9008 (2007). doi: 10.1523/JNEUROSCI.1717-07.2007; pmid: 17715337
8. D. Ledergerber, M. E. Larkum, Properties of layer 6 pyramidal neuron apical dendrites. *J. Neurosci.* **30**, 13031–13044 (2010). doi: 10.1523/JNEUROSCI.2254-10.2010; pmid: 20881121
9. N. L. Golding, N. Spruston, Dendritic sodium spikes are variable triggers of axonal action potentials in hippocampal CA1 pyramidal neurons. *Neuron* **21**, 1189–1200 (1998). doi: 10.1016/S0896-6273(00)80635-2; pmid: 9856473
10. N. L. Golding, N. P. Staff, N. Spruston, Dendritic spikes as a mechanism for cooperative long-term potentiation. *Nature* **418**, 326–331 (2002). doi: 10.1038/nature00854; pmid: 12124625
11. Y. Kim, C.-L. Hsu, M. S. Cembrowski, B. D. Mensh, N. Spruston, Dendritic sodium spikes are required for long-term potentiation at distal synapses on hippocampal pyramidal neurons. *eLife* **4**, e06414 (2015). doi: 10.7554/eLife.06414; pmid: 26247712
12. B. A. Milojkovic, J. P. Wuskell, L. M. Loew, S. D. Antic, Initiation of sodium spikelets in basal dendrites of neocortical pyramidal neurons. *J. Membr. Biol.* **208**, 155–169 (2005). doi: 10.1007/s00232-005-0827-7; pmid: 16645744
13. H. G. Kim, B. W. Connors, Apical dendrites of the neocortex: Correlation between sodium- and calcium-dependent spiking and pyramidal cell morphology. *J. Neurosci.* **13**, 5301–5311 (1993). pmid: 8254376
14. S. Remy, N. Spruston, Dendritic spikes induce single-burst long-term potentiation. *Proc. Natl. Acad. Sci. U.S.A.* **104**, 17192–17197 (2007). doi: 10.1073/pnas.0707919104; pmid: 17940015
15. A. Losonczy, J. K. Makara, J. C. Magee, Compartmentalized dendritic plasticity and input feature storage in neurons. *Nature* **452**, 436–441 (2008). doi: 10.1038/nature06725; pmid: 18368112
16. S. Remy, J. Csicsvari, H. Beck, Activity-dependent control of neuronal output by local and global dendritic spike attenuation. *Neuron* **61**, 906–916 (2009). doi: 10.1016/j.neuron.2009.01.032; pmid: 19323999
17. G. J. Stuart, B. Sakmann, Active propagation of somatic action potentials into neocortical pyramidal cell dendrites. *Nature* **367**, 69–72 (1994). doi: 10.1038/367069a0; pmid: 8107777
18. C. M. Colbert, J. C. Magee, D. A. Hoffman, D. Johnston, Slow recovery from inactivation of Na^+ channels underlies the activity-dependent attenuation of dendritic action potentials in hippocampal CA1 pyramidal neurons. *J. Neurosci.* **17**, 6512–6521 (1997). pmid: 9254663
19. N. L. Golding, W. L. Kath, N. Spruston, Dichotomy of action-potential backpropagation in CA1 pyramidal neuron dendrites. *J. Neurophysiol.* **86**, 2998–3010 (2001). pmid: 11731556
20. M. E. Larkum, J. J. Zhu, Signaling of layer 1 and whisker-evoked Ca^{2+} and Na^+ action potentials in distal and terminal dendrites of rat neocortical pyramidal neurons in vitro and in vivo. *J. Neurosci.* **22**, 6991–7005 (2002). pmid: 12177197
21. J. Waters, M. Larkum, B. Sakmann, F. Helmchen, Supralinear Ca^{2+} influx into dendritic tufts of layer 2/3 neocortical pyramidal neurons in vitro and in vivo. *J. Neurosci.* **23**, 8558–8567 (2003). pmid: 13679425
22. M. E. Larkum, J. J. Zhu, B. Sakmann, A new cellular mechanism for coupling inputs arriving at different cortical layers. *Nature* **398**, 338–341 (1999). doi: 10.1038/18686; pmid: 10192334
23. R. Llinas, C. Nicholson, Electrophysiological properties of dendrites and somata in alligator Purkinje cells. *J. Neurophysiol.* **34**, 532–551 (1971). pmid: 4329778
24. H. Pockberger, Electrophysiological and morphological properties of rat motor cortex neurons in vivo. *Brain Res.* **539**, 181–190 (1991). doi: 10.1016/0006-8993(91)91619-C; pmid: 1711391
25. A. Kamondi, L. Acsády, G. Buzsáki, Dendritic spikes are enhanced by cooperative network activity in the intact hippocampus. *J. Neurosci.* **18**, 3919–3928 (1998). pmid: 9570819
26. S. L. Smith, I. T. Smith, T. Branco, M. Häusser, Dendritic spikes enhance stimulus selectivity in cortical neurons in vivo. *Nature* **503**, 115–120 (2013). doi: 10.1038/nature12600; pmid: 24162850
27. J. C. Magee, D. Johnston, Characterization of single voltage-gated Na^+ and Ca^{2+} channels in apical dendrites of rat CA1 pyramidal neurons. *J. Physiol.* **487**, 67–90 (1995). doi: 10.1113/jphysiol.1995.sp020862; pmid: 7473260
28. J. S. Nettleton, W. J. Spain, Linear to supralinear summation of AMPA-mediated EPSPs in neocortical pyramidal neurons. *J. Neurophysiol.* **83**, 3310–3322 (2000). pmid: 10848551
29. A. Reyes, Influence of dendritic conductances on the input-output properties of neurons. *Annu. Rev. Neurosci.* **24**, 653–675 (2001). doi: 10.1146/annurev.neuro.24.1.653; pmid: 11520915
30. D. Johnston, J. C. Magee, C. M. Colbert, B. R. Cristie, Active properties of neuronal dendrites. *Annu. Rev. Neurosci.* **19**, 165–186 (1996). doi: 10.1146/annurev.ne.19.030196.001121; pmid: 8833440
31. N. Spruston, Pyramidal neurons: Dendritic structure and synaptic integration. *Nat. Rev. Neurosci.* **9**, 206–221 (2008). doi: 10.1038/nrn2286; pmid: 18270515
32. R. Yuste, D. W. Tank, Dendritic integration in mammalian neurons, a century after Cajal. *Neuron* **16**, 701–716 (1996). doi: 10.1016/S0896-6273(00)80091-4; pmid: 8607989
33. D. Johnston, R. Narayanan, Active dendrites: Colorful wings of the mysterious butterflies. *Trends Neurosci.* **31**, 309–316 (2008). doi: 10.1016/j.tins.2008.03.004; pmid: 18471907
34. B. W. Mel, Synaptic integration in an excitable dendritic tree. *J. Neurophysiol.* **70**, 1086–1101 (1993). pmid: 8229160
35. M. Häusser, B. Mel, Dendrites: Bug or feature? *Curr. Opin. Neurobiol.* **13**, 372–383 (2003). doi: 10.1016/S0959-4388(03)00075-8; pmid: 12850223
36. M. R. Mehta, Cooperative LTP can map memory sequences on dendritic branches. *Trends Neurosci.* **27**, 69–72 (2004). doi: 10.1016/j.tins.2003.12.004; pmid: 15106650
37. M. London, M. Häusser, Dendritic computation. *Annu. Rev. Neurosci.* **28**, 503–532 (2005). doi: 10.1146/annurev.neuro.28.061604.135703; pmid: 16033324
38. A. Kumar, M. R. Mehta, Frequency-dependent changes in NMDAR-dependent synaptic plasticity. *Front. Comput. Neurosci.* **5**, 38 (2011). doi: 10.3389/fncom.2011.00038; pmid: 21994493
39. F. Helmchen, K. Svoboda, W. Denk, D. W. Tank, In vivo dendritic calcium dynamics in deep-layer cortical pyramidal neurons. *Nat. Neurosci.* **2**, 989–996 (1999). doi: 10.1038/14788; pmid: 10526338
40. M. Murayama *et al.*, Dendritic encoding of sensory stimuli controlled by deep cortical interneurons. *Nature* **457**, 1137–1141 (2009). doi: 10.1038/nature07663; pmid: 19151696
41. B. Sakmann, E. Neher, Patch clamp techniques for studying ionic channels in excitable membranes. *Annu. Rev. Physiol.* **46**, 455–472 (1984). doi: 10.1146/annurev.ph.46.030184.002323; pmid: 6143532
42. M. R. DeWeese, Whole-cell recording in vivo. *Curr. Protoc. Neurosci.* **Chapter 6**, Unit 6.22 (2007). doi: 10.1002/0471142301.ns0622s38; pmid: 18428661
43. P. Alcami, R. Franconville, I. Llano, A. Marty, Measuring the firing rate of high-resistance neurons with cell-attached recording. *J. Neurosci.* **32**, 3118–3130 (2012). doi: 10.1523/JNEUROSCI.5371-11.2012; pmid: 22378885
44. J. S. Gillespie, The electrical and mechanical responses of intestinal smooth muscle cells to stimulation of their extrinsic parasympathetic nerves. *J. Physiol.* **162**, 76–92 (1962). doi: 10.1113/jphysiol.1962.sp006915; pmid: 13898637
45. J. T. McIlwain, O. D. Creutzfeldt, Microelectrode study of synaptic excitation and inhibition in the lateral geniculate nucleus of the cat. *J. Neurophysiol.* **30**, 1–21 (1967).
46. W. Singer, O. D. Creutzfeldt, Reciprocal lateral inhibition of on- and off-center neurones in the lateral geniculate body of the cat. *Exp. Brain Res.* **10**, 311–330 (1970). doi: 10.1007/BF00235054; pmid: 4315066
47. A. M. L. Coenen, A. J. H. Vendrik, Determination of the transfer ratio of cat's geniculate neurons through quasi-intracellular recordings and the relation with the level of alertness. *Exp. Brain Res.* **14**, 227–242 (1972). doi: 10.1007/BF00816160; pmid: 4340696
48. D. M. Finch, E. L. Derian, T. L. Babb, Excitatory projection of the rat subicular complex to the cingulate cortex and synaptic integration with thalamic afferents. *Brain Res.* **301**, 25–37 (1984). doi: 10.1016/0006-8993(84)90399-8; pmid: 6329445
49. W. G. Regehr, J. Pine, C. S. Cohan, M. D. Mischke, D. W. Tank, Sealing cultured invertebrate neurons to embedded dish electrodes facilitates long-term stimulation and recording. *J. Neurosci. Methods* **30**, 91–106 (1989). doi: 10.1016/0165-0270(89)90055-1; pmid: 2586157
50. A. Hai, J. Shappir, M. E. Spira, Long-term, multisite, parallel, in-cell recording and stimulation by an array of

extracellular microelectrodes. *J. Neurophysiol.* **104**, 559–568 (2010). doi: 10.1152/jn.00265.2010; pmid: 20427620
51. P. Ravassard *et al*., Multisensory control of hippocampal spatiotemporal selectivity. *Science* **340**, 1342–1346 (2013). doi: 10.1126/science.1232655; pmid: 23641063
52. Z. M. Aghajan *et al*., Impaired spatial selectivity and intact phase precession in two-dimensional virtual reality. *Nat. Neurosci.* **18**, 121–128 (2015). doi: 10.1038/nn.3884; pmid: 25420065
53. D. H. Szarowski *et al*., Brain responses to micro-machined silicon devices. *Brain Res.* **983**, 23–35 (2003). doi: 10.1016/S0006-8993(03)03023-3; pmid: 12914963
54. V. S. Polikov, P. A. Tresco, W. M. Reichert, Response of brain tissue to chronically implanted neural electrodes. *J. Neurosci. Methods* **148**, 1–18 (2005). doi: 10.1016/j.jneumeth.2005.08.015; pmid: 16198003
55. S. F. Lempka, S. Miocinovic, M. D. Johnson, J. L. Vitek, C. C. McIntyre, In vivo impedance spectroscopy of deep brain stimulation electrodes. *J. Neural Eng.* **6**, 046001 (2009). doi: 10.1088/1741-2560/6/4/046001; pmid: 19494421
56. D. A. Henze *et al*., Intracellular features predicted by extracellular recordings in the hippocampus in vivo. *J. Neurophysiol.* **84**, 390–400 (2000). pmid: 10899213
57. C. Gold, C. C. Girardin, K. A. C. Martin, C. Koch, High-amplitude positive spikes recorded extracellularly in cat visual cortex. *J. Neurophysiol.* **102**, 3340–3351 (2009). doi: 10.1152/jn.91365.2008; pmid: 19793873
58. J. C. Williams, J. A. Hippensteel, J. Dilgen, W. Shain, D. R. Kipke, Complex impedance spectroscopy for monitoring tissue responses to inserted neural implants. *J. Neural Eng.* **4**, 410–423 (2007). doi: 10.1088/1741-2560/4/4/007; pmid: 18057508
59. C. D. Harvey, F. Collman, D. A. Dombeck, D. W. Tank, Intracellular dynamics of hippocampal place cells during virtual navigation. *Nature* **461**, 941–946 (2009). doi: 10.1038/nature08499; pmid: 19829374
60. A. K. Lee, I. D. Manns, B. Sakmann, M. Brecht, Whole-cell recordings in freely moving rats. *Neuron* **51**, 399–407 (2006). doi: 10.1016/j.neuron.2006.07.004; pmid: 16908406
61. M. W. Jones, M. A. Wilson, Theta rhythms coordinate hippocampal-prefrontal interactions in a spatial memory task. *PLOS Biol.* **3**, e402 (2005). doi: 10.1371/journal.pbio.0030402; pmid: 16279838
62. O. P. Hamill, J. R. Huguenard, D. A. Prince, Patch-clamp studies of voltage-gated currents in identified neurons of the rat cerebral cortex. *Cereb. Cortex* **1**, 48–61 (1991). doi: 10.1093/cercor/1.1.48; pmid: 1668364
63. T. J. McHugh, K. I. Blum, J. Z. Tsien, S. Tonegawa, M. A. Wilson, Impaired hippocampal representation of space in CA1-specific NMDAR1 knockout mice. *Cell* **87**, 1339–1349 (1996). doi: 10.1016/S0092-8674(00)81828-0; pmid: 8980239
64. E. Resnik, J. M. McFarland, R. Sprengel, B. Sakmann, M. R. Mehta, The effects of GluA1 deletion on the hippocampal population code for position. *J. Neurosci.* **32**, 8952–8968 (2012). doi: 10.1523/JNEUROSCI.6460-11.2012; pmid: 22745495
65. K. M. M. Kaiser, Y. Zilberter, B. Sakmann, Back-propagating action potentials mediate calcium signalling in dendrites of bitufted interneurons in layer 2/3 of rat somatosensory cortex. *J. Physiol.* **535**, 17–31 (2001). doi: 10.1111/j.1469-7793.2001.t01-1-00017.x; pmid: 11507155
66. F. Saraga, C. P. Wu, L. Zhang, F. K. Skinner, Active dendrites and spike propagation in multi-compartment models of oriens-lacunosum/moleculare hippocampal interneurons. *J. Physiol.* **552**, 673–689 (2003). doi: 10.1113/jphysiol.2003.046177; pmid: 12923216
67. C. Gold, D. A. Henze, C. Koch, G. Buzsáki, On the origin of the extracellular action potential waveform: A modeling study. *J. Neurophysiol.* **95**, 3113–3128 (2006). doi: 10.1152/jn.00979.2005; pmid: 16467426
68. R. J. Douglas, K. A. C. Martin, Neuronal circuits of the neocortex. *Annu. Rev. Neurosci.* **27**, 419–451 (2004). doi: 10.1146/annurev.neuro.27.070203.144152; pmid: 15217339
69. M. Almog, A. Korngreen, A quantitative description of dendritic conductances and its application to dendritic excitation in layer 5 pyramidal neurons. *J. Neurosci.* **34**, 182–196 (2014). doi: 10.1523/JNEUROSCI.2896-13.2014; pmid: 24381280
70. M. L. Hines, N. T. Carnevale, Neuron: A tool for neuroscientists. *Neuroscientist* **7**, 123–135 (2001). doi: 10.1177/107385840100700207; pmid: 11496923
71. A. Destexhe, M. Rudolph, J.-M. Fellous, T. J. Sejnowski, Fluctuating synaptic conductances recreate in vivo-like activity in neocortical neurons. *Neuroscience* **107**, 13–24 (2001). doi: 10.1016/S0306-4522(01)00344-X; pmid: 11744242
72. A. Destexhe, M. Rudolph, D. Paré, The high-conductance state of neocortical neurons in vivo. *Nat. Rev. Neurosci.* **4**, 739–751 (2003). doi: 10.1038/nrn1198; pmid: 12951566
73. G. E. Uhlenbeck, L. S. Ornstein, On the theory of the Brownian motion. *Phys. Rev.* **36**, 823–841 (1930). doi: 10.1103/PhysRev.36.823
74. C. C. H. Petersen, T. T. G. Hahn, M. Mehta, A. Grinvald, B. Sakmann, Interaction of sensory responses with spontaneous depolarization in layer 2/3 barrel cortex. *Proc. Natl. Acad. Sci. U.S.A.* **100**, 13638–13643 (2003). doi: 10.1073/pnas.2235811100; pmid: 14595013
75. R. Azouz, C. M. Gray, Dynamic spike threshold reveals a mechanism for synaptic coincidence detection in cortical neurons in vivo. *Proc. Natl. Acad. Sci. U.S.A.* **97**, 8110–8115 (2000). doi: 10.1073/pnas.130200797; pmid: 10859358
76. C. M. Constantinople, R. M. Bruno, Effects and mechanisms of wakefulness on local cortical networks. *Neuron* **69**, 1061–1068 (2011). doi: 10.1016/j.neuron.2011.02.040; pmid: 21435553
77. S. Chauvette, S. Crochet, M. Volgushev, I. Timofeev, Properties of slow oscillation during slow-wave sleep and anesthesia in cats. *J. Neurosci.* **31**, 14998–15008 (2011). doi: 10.1523/JNEUROSCI.2339-11.2011; pmid: 22016533
78. J. R. Whitlock, G. Pfuhl, N. Dagslott, M.-B. Moser, E. I. Moser, Functional split between parietal and entorhinal cortices in the rat. *Neuron* **73**, 789–802 (2012). doi: 10.1016/j.neuron.2011.12.028; pmid: 22365551
79. D. A. Nitz, Tracking route progression in the posterior parietal cortex. *Neuron* **49**, 747–756 (2006). doi: 10.1016/j.neuron.2006.01.037; pmid: 16504949
80. T. W. Margrie, M. Brecht, B. Sakmann, In vivo, low-resistance, whole-cell recordings from neurons in the anaesthetized and awake mammalian brain. *Pflugers Arch.* **444**, 491–498 (2002). doi: 10.1007/s00424-002-0831-z; pmid: 12136268
81. D. Lee, B.-J. Lin, A. K. Lee, Hippocampal place fields emerge upon single-cell manipulation of excitability during behavior. *Science* **337**, 849–853 (2012). doi: 10.1126/science.1221489; pmid: 22904011
82. C. Schmidt-Hieber, M. Häusser, Cellular mechanisms of spatial navigation in the medial entorhinal cortex. *Nat. Neurosci.* **16**, 325–331 (2013). doi: 10.1038/nn.3340; pmid: 23396102
83. C. Lenschow, M. Brecht, Barrel cortex membrane potential dynamics in social touch. *Neuron* **85**, 718–725 (2015). doi: 10.1016/j.neuron.2014.12.059; pmid: 25640075
84. R. Linsker, Neural network learning of optimal Kalman prediction and control. *Neural Netw.* **21**, 1328–1343 (2008). doi: 10.1016/j.neunet.2008.05.002; pmid: 18602247
85. S. Deneve, Bayesian spiking neurons I: Inference. *Neural Comput.* **20**, 91–117 (2008). doi: 10.1162/neco.2008.20.1.118; pmid: 18045002
86. M. R. Mehta, M. C. Quirk, M. A. Wilson, Experience-dependent asymmetric shape of hippocampal receptive fields. *Neuron* **25**, 707–715 (2000). doi: 10.1016/S0896-6273(00)81072-7; pmid: 10774737
87. M. R. Mehta, From synaptic plasticity to spatial maps and sequence learning. *Hippocampus* **25**, 756–762 (2015). doi: 10.1002/hipo.22472; pmid: 25929239
88. N. K. Logothetis, B. A. Wandell, Interpreting the BOLD signal. *Annu. Rev. Physiol.* **66**, 735–769 (2004). doi: 10.1146/annurev.physiol.66.082602.092845; pmid: 14977420
89. E. Schneidman, M. J. Berry II, R. Segev, W. Bialek, Weak pairwise correlations imply strongly correlated network states in a neural population. *Nature* **440**, 1007–1012 (2006). doi: 10.1038/nature04701; pmid: 16625187

ACKNOWLEDGMENTS

We thank Z. M. Aghajan and K. Safaryan for useful discussions on analysis techniques, D. Aharoni and B. Willers for help with electrophysiology, M. Cilluffo (University of California, Los Angeles, Brain Research Institute Microscopic Techniques Core) for immunohistochemical services, P. Chen for confocal microscopy, and F. Schweizer and I. Mody for discussion and careful reading of the manuscript. Portions of these results were presented at the annual Society for Neuroscience meetings in 2012, 2013, and 2014.

SUPPLEMENTARY MATERIALS

www.sciencemag.org/content/355/6331/eaaj1497/suppl/DC1
Materials and Methods
Figs. S1 to S12
Table S1
Movies S1 and S2

3 September 2016; accepted 31 January 2017
Published online 9 March 2017
10.1126/science.aaj1497

Dynamics of cortical dendritic membrane potential and spikes in freely behaving rats

Jason J. Moore, Pascal M. Ravassard, David Ho, Lavanya Acharya, Ashley L. Kees, Cliff Vuong and Mayank R. Mehta

Science **355** (6331), eaaj1497.
DOI: 10.1126/science.aaj1497originally published online March 9, 2017

Dendrites are more active than expected

Dendrites occupy more than 90% of neuronal tissue. However, it has not been possible to measure distal dendritic membrane potential and spiking in vivo over a long period of time. Moore *et al.* developed a technique to record the subthreshold membrane potential and spikes from neocortical distal dendrites in freely behaving animals. These recordings were very stable, providing data from a single dendrite for up to 4 days. Unexpectedly, distal dendrites generated action potentials whose firing rate was nearly five times greater than at the cell body.

Science, this issue p. eaaj1497